Electronic Supplementary Material (ESI) for Chemical Communications

Electrocatalytic reduction of CO_2 to CO by polypyridyl ruthenium complexes

Zuofeng Chen, Chuncheng Chen, David R. Weinberg, Peng Kang, Javier J. Concepcion, Daniel P. Harrison, Maurice S. Brookhart, and Thomas J. Meyer*

Department of Chemistry, University of North Carolina at Chapel Hill, Chapel Hill, NC, 27599, USA

Supporting Information

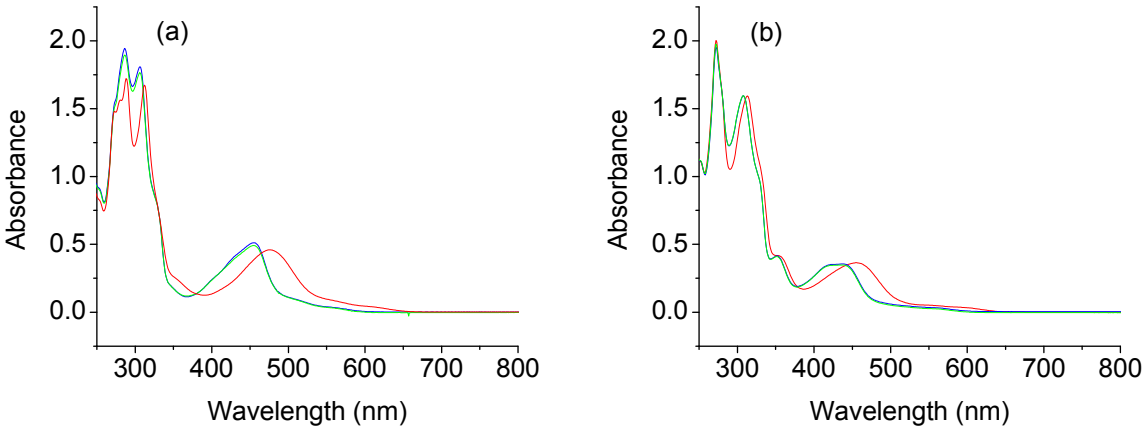

Figure S1. (a) UV-visible spectra of 50 μM $[Ru(tpy)(bpy)(S)]^{2+}$ **1** in H_2O (red line, as $[Ru(tpy)(bpy)(H_2O)]^{2+}$), CH_3CN (blue line, as $[Ru(tpy)(bpy)(NCCH_3)]^{2+}$), and 10% (v/v)

H_2O/CH_3CN (green line, as $[Ru(tpy)(bpy)(NCCH_3)]^{2+}$). Note the blue and green lines are overlaid. (b) as in (a) with $[Ru(tpy)(Mebim\text{-}py)(S)]^{2+}$ **2**.

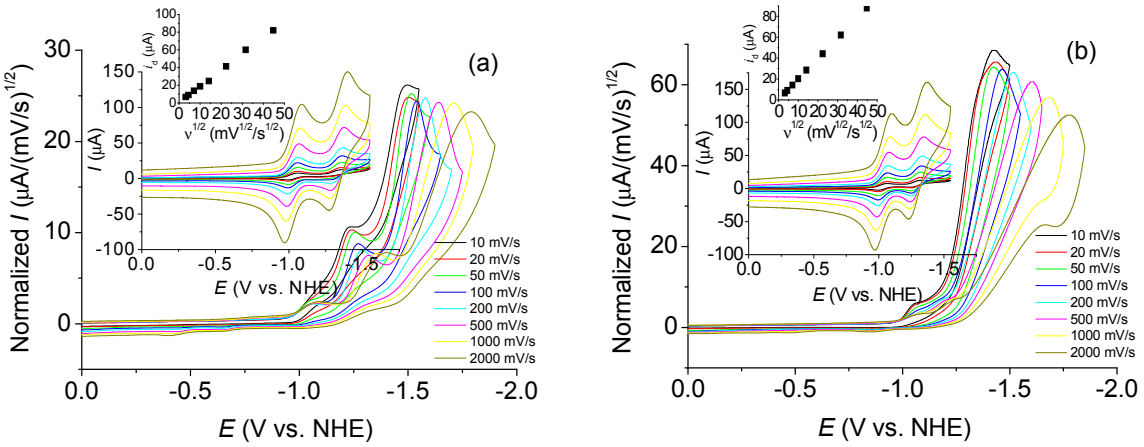

Figure S2. Scan rate normalized ($i/v^{1/2}$) cyclic voltammograms of 1 mM **1** (a) and **2** (b) in 0.1 M $^{n}Bu_4NPF_6/CH_3CN$ under CO_2 at different scan rates. Insets (without normalization) as in the main figures but under Ar, and plots of i_d for the first reduction peak current vs the square root of the scan rate ($v^{1/2}$). Electrode, glassy carbon.

The behavior of complexes **1** and **2** under Ar is governed by Randles-Sevcik equation, $i_d = 0.4463nFA[Ru](nFvD_{Ru}/RT)^{1/2}$. From the plots of i_d vs $v^{1/2}$ in the insets and Randles-Sevcik equation, D_{Ru}, the catalyst diffusion coefficient, was calculated to be ~5.2×10^{-6} cm^2/s.

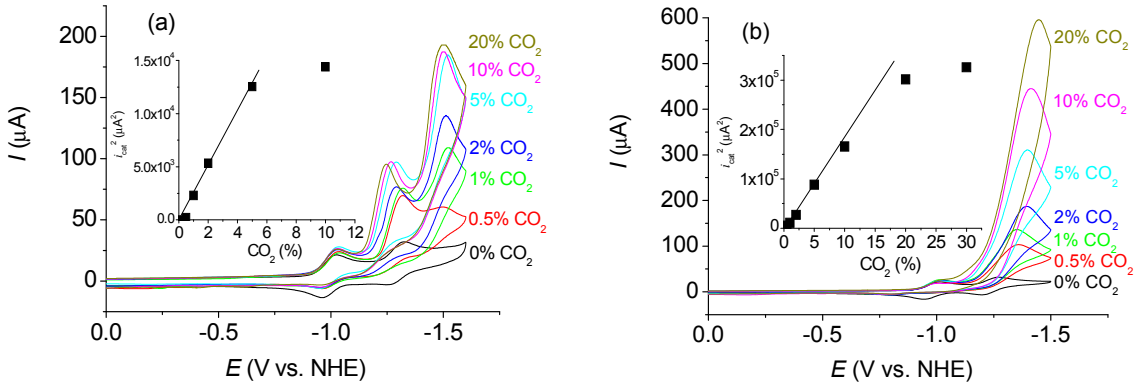

Figure S3. Cyclic voltammograms of 1 mM catalyst **1** (a) and **2** (b) in 0.1 M $^{n}Bu_4NPF_6/CH_3CN$ with increasing concentrations of CO_2 in CO_2/Ar mixtures. Insets show plots of i_{cat}^2 at the catalytic peak potential at $E_{p,c}$ = −1.52 V (a) and −1.46 V (b) vs [CO_2] in CO_2/Ar mixtures. Electrode, glassy carbon; scan rate, 100 mV/s.

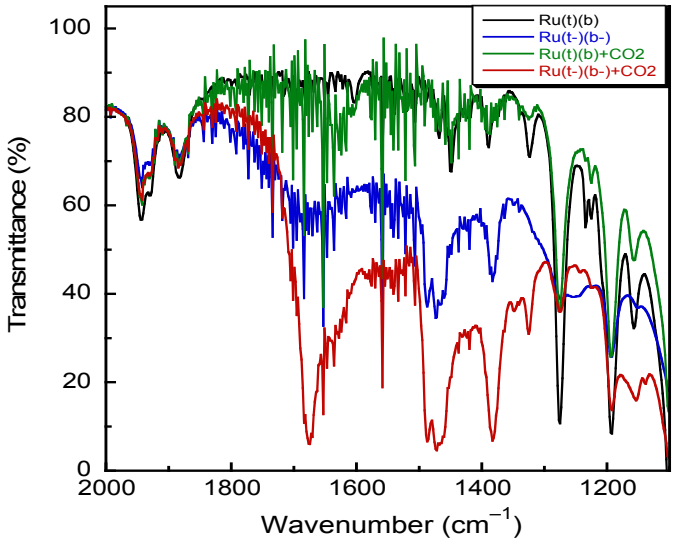

Figure S4. FT-IR spectra of **1** (black line, as $[(tpy)(bpy)Ru^{II}(S)]^{2+}$), doubly reduced **1** (blue line, as $[(tpy^{-})(bpy^{-})Ru^{II}(S)]^{0}$), and doubly reduced **1** followed by addition of CO_2 (red line, as $[(tpy)(bpy)Ru^{II}(CO_2)^{2-}]^{0}$). Doubly reduced **1** was generated by electrolysis at a vitreous carbon electrode with potential held at –1.34 V vs NHE (0.1 M $^{n}Bu_4NPF_6$, CH_3CN) under Ar

atmosphere. Upon generation of doubly reduced **1**, the headspace of the electrolysis cell was gently purged with CO_2. The appearance of a ν(COO^-) stretch at 1675 cm^{-1} in the spectrum shown in red is consistent with formation of the metallocarboxylate intermediate $[(tpy)(bpy)Ru^{II}(CO_2^{2-})]^0$ formed by addition of CO_2 to doubly reduced **1**. For comparison, addition of CO_2 to a solution of **1**, green spectrum, results in no spectral difference.

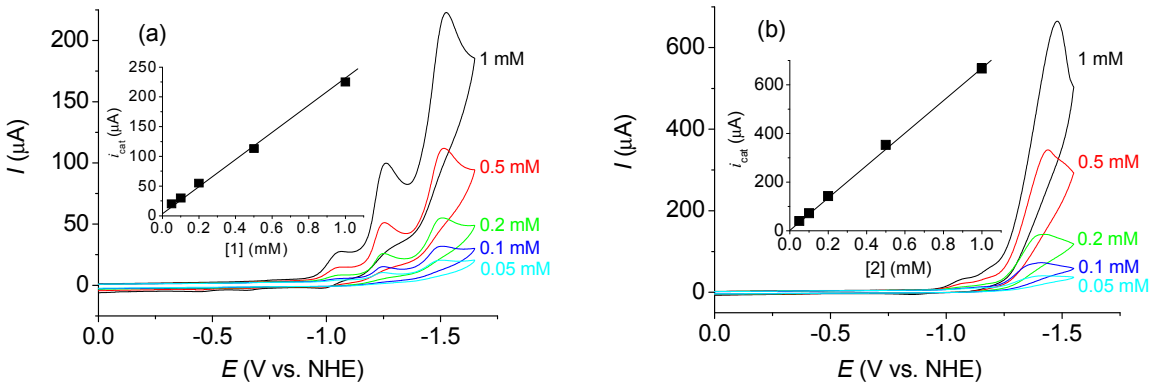

Figure S5. Cyclic voltammograms at different concentration of **1** (a) and **2** (b) in 0.1 M $^nBu_4NPF_6/CH_3CN$ under CO_2. Insets show plots of i_{cat} at the catalytic peak potential at $E_{p,c}$= –1.52 V (a) and –1.46 V (b) vs [Ru]. Electrode, glassy carbon; scan rate, 100 mV/s.

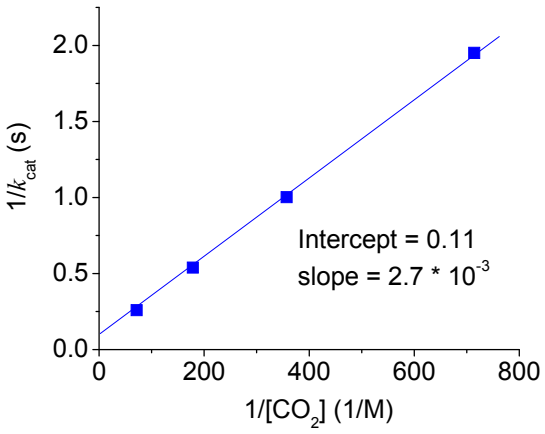

Figure S6. As in Figure 3, plot of $1/k_{cat}$ vs $1/[CO_2]$. k_{cat} was calculated from eq 3a. According to eq 5b, from the intercept ($1/k_D$), $k_D = 9\ s^{-1}$ and from the intercept-to-slope ratio (k_{CO2}/k_{-D}), $k_{CO2}/k_{-D} = 40\ M^{-1}$.

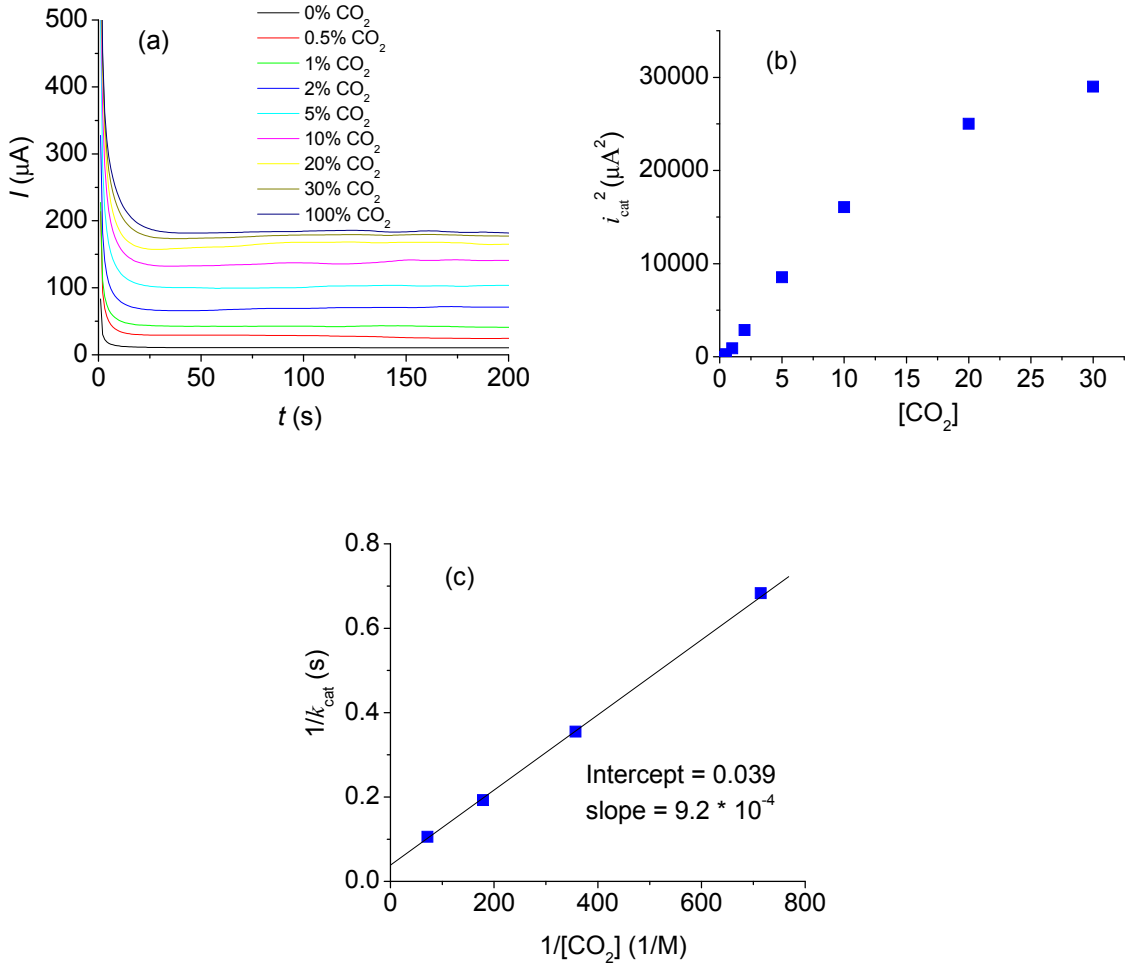

Figure S7. (a) Controlled potential electrolysis of 1 mM **2** in 0.1 M $^{n}Bu_4NPF_6/CH_3CN$ (unstirred) with increasing concentrations of CO_2 in CO_2/Ar mixtures at a glassy carbon electrode (0.071cm^2) at –1.46 V. (b) Plot of i_{cat}^2 (background current subtracted) vs $[CO_2]$ in CO_2/Ar mixtures. (c) Plot of $1/k_{cat}$ vs $1/[CO_2]$. k_{cat} was calculated from eq 3a. According to eq

5b, from the intercept ($1/k_D$), k_D = 26 s^{-1} and from the intercept-to-slope ratio (k_{CO2}/k_{-D}), k_{CO2}/k_{-D} = 43 M^{-1}.

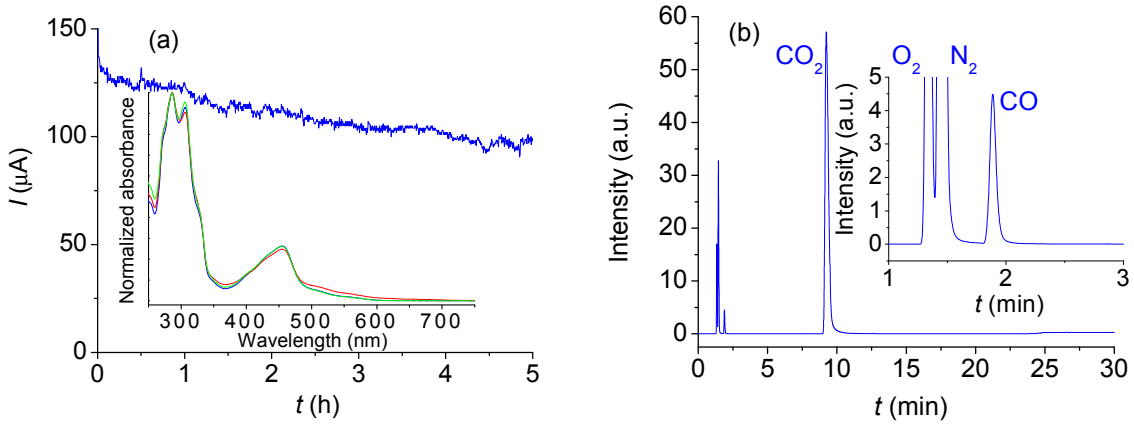

Figure S8. (a) Controlled potential electrolysis of 1 mM **1** at –1.52 V in CO_2 saturated 0.1 M $^nBu_4NPF_6/CH_3CN$ at a glassy carbon electrode (0.071 cm^2). The solution was stirred during electrolysis. Inset shows UV-visible spectra of **1** before (blue line) and after (red line) electrolysis and after addition of acid at the end of the electrolysis period (green line). Note the slight decrease at 455 nm and increase at 485-600 nm in the red line consistent with possible anation in the shift of the lowest energy MLCT absorption to lower energy. (b) The corresponding gas chromatogram after electrolysis. The inset shows a magnified view in the initial 3 min.

Over extended electrolysis periods, as HCO_3^-/CO_3^{2-} builds up in solution, the electrolysis current gradually falls due to the buildup of a precipitate on the electrode with the solution color gradually turning to purple. These observations are consistent with precipitation of the catalyst as the CO_3^{2-} salt and coordination of HCO_3^-/CO_3^{2-} to give the carbonate or bicarbonate complexes possibly as $[Ru(tpy)(bpy)(OC(O)O)]^0$ or $[Ru(tpy)(bpy)(OC(O)OH)]^+$. Addition of dilute $HClO_4$

or HNO_3 regenerates the UV-visible spectrum of the catalyst quantitatively, Figure S8a inset, and restores electrocatalytic activity.

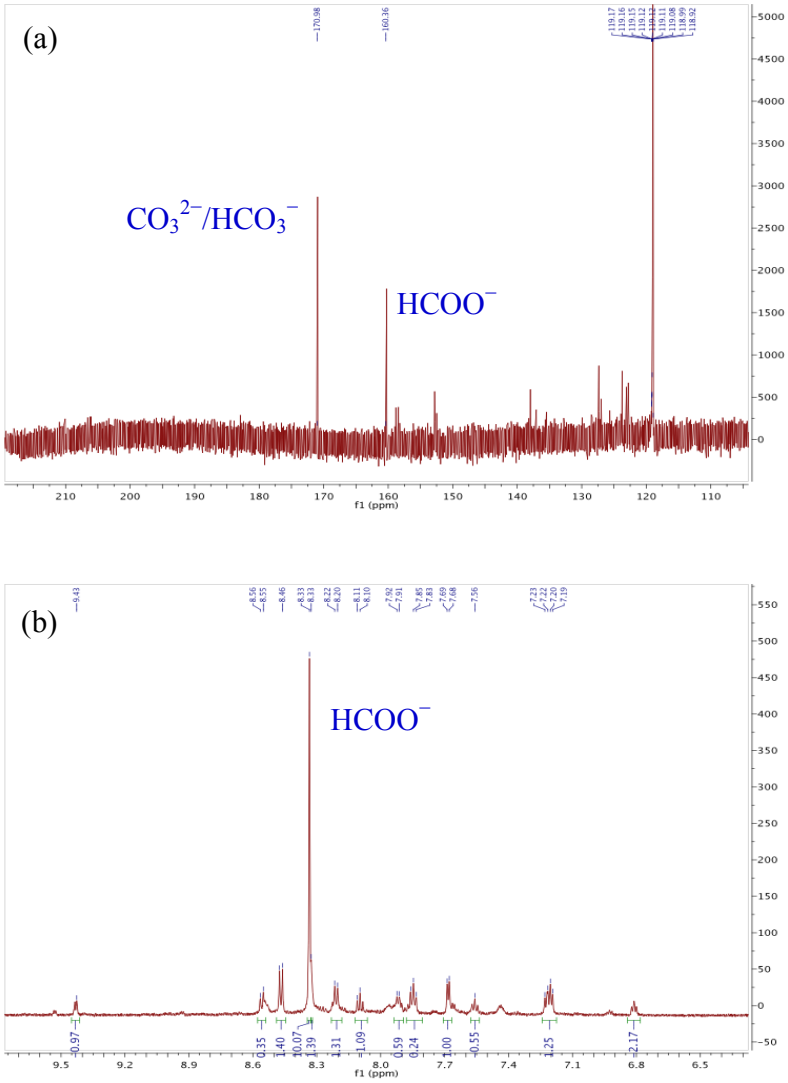

Figure S9. (a) ^{13}C NMR spectrum showing resonances for CO_3^{2-}/HCO_3^- and $HCOO^-$ as co-products after electrolysis under CO_2 (Note that normal CO_2 and not ^{13}C enriched CO_2 was used in the ^{13}C NMR experiment.). In a control experiment, there was no evidence in ^{13}C spectra for CO_3^{2-}/HCO_3^- or $HCOO^-$ resonances before electrolysis under the same experimental conditions. (b) ^1H NMR spectrum showing the $HCOO^-$ resonance obtained after electrolysis under CO_2. A

vitreous carbon electrode was used for the electrolysis at −1.52 V vs NHE in solution 1 mM in **1** in 0.1 M $^{n}Bu_4NPF_6/CH_3CN$.

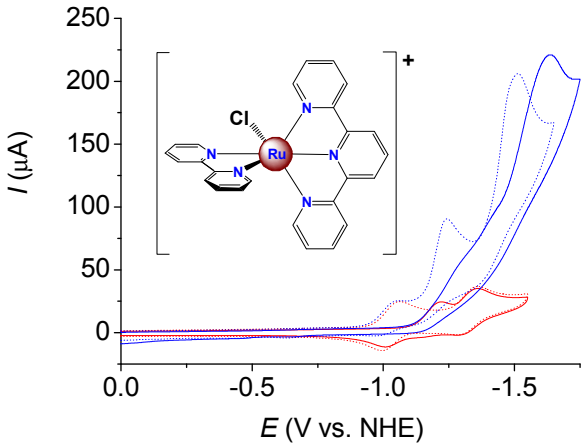

Figure S10. Cyclic voltammograms of 1 mM $[Ru(tpy)(bpy)(Cl)]^{+}$ (Inset shows its structure) in 0.1 M $^{n}Bu_4NPF_6/CH_3CN$ under Ar (red line) and CO_2 (blue line). The dotted lines are the CVs of $[Ru(tpy)(bpy)(NCCH_3)]^{2+}$ under the same conditions for comparison. Electrode, glassy carbon; scan rate, 100 mV/s. Under Ar, $E_{p,c}$ for the first tpy reduction of $[Ru(tpy)(bpy)(Cl)]^{+}$ is shifted by −0.18 V relative to $[Ru(tpy)(bpy)(NCCH_3)]^{2+}$ largely due to the decrease in charge. Following tpy reduction, the bpy-based reduction occurs at the same potential as in $[Ru(tpy)(bpy)(NCCH_3)]^{2+}$ pointing to loss of Cl^{-} and substitution by CH_3CN solvent.

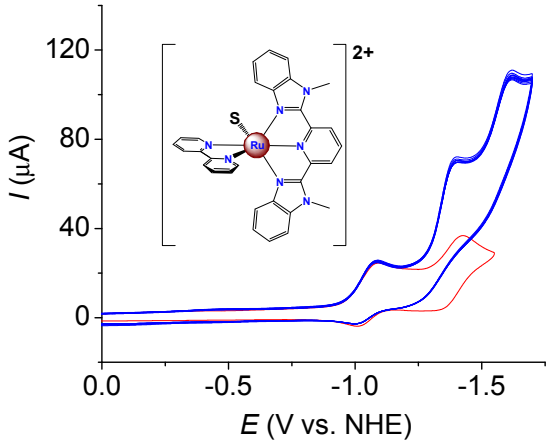

Figure S11. Cyclic voltammograms of 1 mM $[Ru(Mebimpy)(bpy)(S)]^{2+}$ (Inset shows its structure) in 0.1 M $^{n}Bu_4NPF_6/CH_3CN$ under Ar (red line) and CO_2 (blue line, 10 successive scan cycles). Electrode, glassy carbon; scan rate, 100 mV/s.

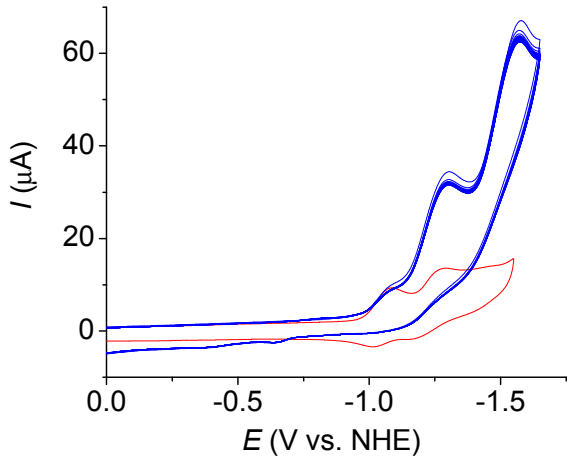

Figure S12. Cyclic voltammograms of 1 mM **1** in 0.1 M $^{n}Bu_4NPF_6$/PC under Ar (red line) and CO_2 (blue line, 25 successive scan cycles). Electrode, glassy carbon; scan rate, 100 mV/s.

DFT calculations: The geometric optimization and electronic structures were obtained at the ub3lyp/lanl2dz level with the Gaussian 03 (G03) program package.[1]

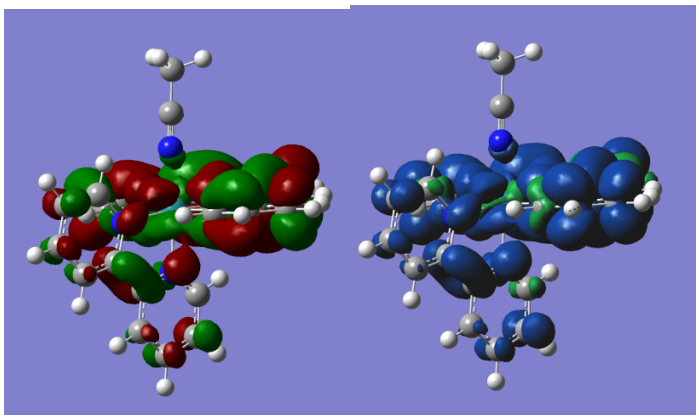

Figure DFT1. Singly occupied molecular orbital (SOMO) (left) and total spin density (TSD) (right) for $1e^-$ reduced $[Ru(tpy)(bpy)(NCCH_3)]^+$. Both SOMO and TSD are mainly spread over the tpy ring, indicating that the first reduction occurs at the tpy ligand.

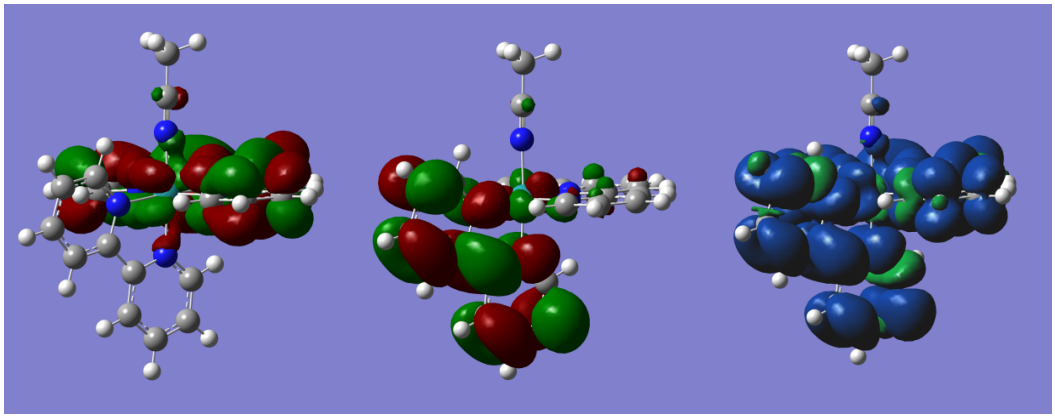

Figure DFT2. HOMO-1(left), HOMO (middle) orbitals, and TSD (right) for the $2e^-$ reduced complex $^3[Ru(tpy)(bpy)(CH_3CN)]^0$. The $2e^-$ reduced $[Ru(tpy)(bpy)(CH_3CN)]^0$ complex has two possible electronic configurations: (1)The two added electrons are paired and both are distributed over the tpy ring, i.e., the complex is in the singlet state, $^1[Ru(tpy)(bpy)(CH_3CN)]^0$. (2) The

second electronis added to the bpy ring, i.e., the complex is in the triplet state, $^3[Ru(tpy)(bpy)(CH_3CN)]^0$. The calculated energy for the electron-paired singlet complex is ~85.1 kcal/mol higher than the triplet favoring the triplet as the ground state. The electronic structures here indicate that, upon two electron reduction, the electrons enter π* orbitals of the tpy ring and the bpy ring, respectively. Accordingly, the spin density of $^3[Ru(tpy)(bpy)(CH_3CN)]^0$ is distributed on both tpy and bpy rings.

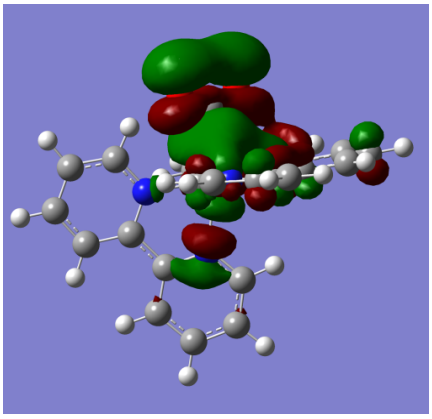

Figure DFT3. HOMO for $[Ru(tpy)(bpy)(CO_2)]^0$. In contrast to $[Ru(tpy)(bpy)(NCCH_3)]^0$ complex, the singlet state of the $2e^-$ reduced $[Ru(tpy)(bpy)(CO_2)]^0$ complex is more stable than the triplet by ~9 kcal/mol. The HOMO for $[Ru(tpy)(bpy)(CO_2)]^0$ is located at the coordinated CO_2, consistent with the formulation $[Ru^{II}(tpy)(bpy)(CO_2^{2-})]^0$ and the internal $2e^-$ transfer reaction shown in eq 1c with internal electron from the tpy and bpy ligands to the coordinated CO_2 when CH_3CN is substituted by CO_2 in the $2e^-$ reduced complex.

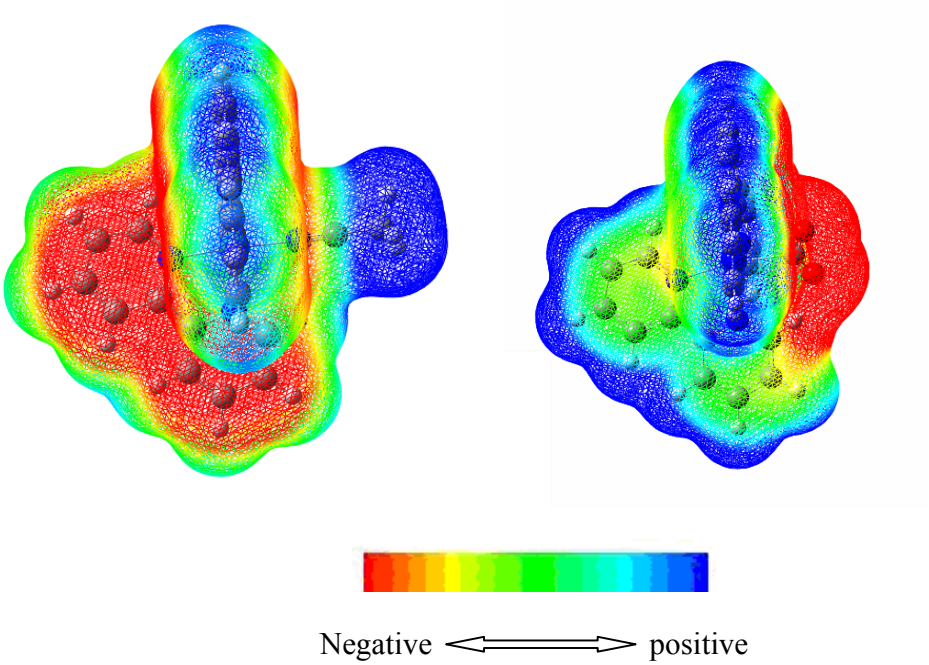

Figure DFT4. The electrostatic potential mapped on the surface of molecular electron density (isodensity, 0.004 e^{-3}) of twice reduced Ru-$NCCH_3$ (left) and Ru-CO_2 (right) complexes. Electrons are distributed on tpy and bpy rings (red area) of Ru-$NCCH_3$ (left), but when the CH_3CN ligand is replaced by CO_2 (right), the electrostatic potential became negative on the CO_2 ligand, indicating the electron move from the tpy and bpy rings to CO_2 after the substitution of CH_3CN by CO_2.

Reference

(1) Gaussian 03 Revision E01. Frisch, M. J.; Trucks, G. W.; Schlegel, H.B.; Scuseria, G. E.; Robb, M. A.; Cheeseman, J. R.; Montgomery, Jr., J.A.; Vreven, T.; Kudin, K. N.; Burant, J. C.; Millam, J. M.; Iyengar, S. S.;Tomasi, J.; Barone, V.; Mennucci, B.; Cossi, M.; Scalmani, G.; Rega,N.; Petersson, G. A.; Nakatsuji, H.; Hada, M.; Ehara, M.; Toyota, K.;Fukuda, R.;

Hasegawa, J.; Ishida, M.; Nakajima, T.; Honda, Y.; Kitao,O.; Nakai, H.; Klene, M.; Li, X.; Knox, J. E.; Hratchian, H. P.; Cross, J.B.; Bakken, V.; Adamo, C.; Jaramillo, J.; Gomperts, R.; Stratmann, R.E.; Yazyev, O.; Austin, A. J.; Cammi, R.; Pomelli, C.; Ochterski, J. W.;Ayala, P. Y.; Morokuma, K.; Voth, G. A.; Salvador, P.; Dannenberg, J.J.; Zakrzewski, V. G.; Dapprich, S.; Daniels, A. D.; Strain, M. C.;Farkas, O.; Malick, D. K.; Rabuck, A. D.; Raghavachari, K.; Foresman,J. B.; Ortiz, J. V.; Cui, Q.; Baboul, A. G.; Clifford, S.; Cioslowski, J.;Stefanov, B. B.; Liu, G.; Liashenko, A.; Piskorz, P.; Komaromi, I.;Martin, R. L.; Fox, D. J.; Keith, T.; Al-Laham, M. A.; Peng, C. Y.;Nanayakkara, A.; Challacombe, M.; Gill, P. M. W.; Johnson, B.; Chen,W.; Wong, M. W.; Gonzalez, C.; and Pople, J. A.; Gaussian, Inc.,Wallingford CT, 2004.